Numerical analyses of the thermal conductivity of random hollow sphere structures

T. Fiedler[1,*], R. Löffler[2], T. Bernthaler[2], R. Winkler[2], I.V. Belova[1], G.E. Murch[1], A. Öchsner[3]

[1]Centre for Mass and Thermal Transport in Engineering Materials, Centre for Geotechnical and Materials Modelling, School of Engineering, The University of Newcastle, Callaghan, NSW 2308, Australia, thomas.fiedler@newcastle.edu.au, irina.belova@newcastle.edu.au, graeme.murch@newcastle.edu.au
[*]Phone +61 2 4921 6208

[2]Department of Surface Engineering and Materials Science, Faculty of Mechanical and Materials Engineering, University Aalen, 73430 Aalen, Germany, ralf.loeffler@htw-aalen.de, timo.bernthaler@htw-aalen.de, ralf.winkler@htw-aalen.de

[3]Department of Applied Mechanics, Faculty of Mechanical Engineering, Technical University of Malaysia, 81310 UTM Skudai, Johor, Malaysia, andreas.oechsner@gmail.com

Abstract

This paper presents Lattice Monte Carlo (LMC) and Finite Element (FE) analyses on the effective thermal conductivity of sintered Metallic Hollow Spheres Structures (MHSS). A novel analysis technique applying LMC permits the utilisation of large high resolution models and can be based on computed tomography (CT) images. As a consequence, simulations are performed using the real geometry and no simplifications, such as the use of model structures, need to be introduced. In the first part, the influence of the micro-porosity on the effective thermal conductivity of the cell wall material is determined. Using these results, the second part of the analyses directly addresses the thermal properties of sintered MHSS. The findings of the LMC analyses are compared with FE results.

Keywords Thermal properties; Composite materials; Cellular metals; Computer simulation; Porosity

1. Introduction

Well-known advantages of cellular metals are their high ability for energy adsorption [1], good damping behavior [2], sound absorption [3], excellent heat insulation [4] and a high specific stiffness [5]. The combination of these properties opens a wide field of potential applications, e.g. in the automotive, aviation or space industries. However,

despite more than 30 years of intensive scientific research, few industrial applications of these technologies can be found. Essential limiting factors for their utilisation are unevenly distributed material parameters [6] and relatively high production costs. Metallic Hollow-Sphere Structures (MHSS, cf. Fig. 1) are a relatively new group of cellular metals characterised by easily reproducible geometry and therefore more consistent mechanical and physical properties. This paper focuses on the thermal properties of sintered MHSS. These important material characteristics have already been the subject of earlier research. Baumeister and colleagues investigated corundum-based hollow spheres embedded in an epoxy matrix and measured the effective thermal expansion coefficient [7]. It was found that the thermal behaviour of these composites was predominantly governed by the epoxy resin used. Earlier numerical analyses on the thermal properties of MHSS were mostly based on the FE method [8,9]. Within these studies, the numerical model size was limited due to the chosen analysis technique and geometric simplifications needed to be introduced. The real geometry, characterised by a pseudo-random arrangement of hollow spheres, was substituted by cubic symmetric model geometries. In contrast, the LMC method allows the utilisation of large calculation models with high geometric resolution. In [10], two dimensional calculations models representing random cross sections of syntactic MHSS were used in thermal LMC analyses. The current work takes this idea one step further by using CT images as geometrical input data. As a consequence, more accurate results can be obtained. Furthermore, FE meshes are used based on CT data of decreased geometric resolution (cf. Fig. 1c)).

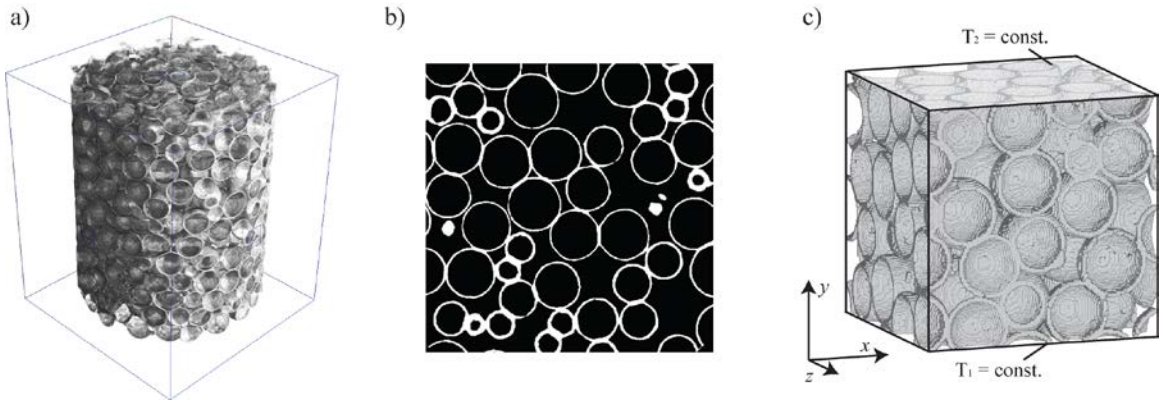

Fig. 1. Geometry of MHSS: a) three dimensional reconstruction of CT data, b) CT cross section used for model generation, c) FE calculation model.

2. Methodology

2.1 Lattice Monte Carlo Analyses

Thermal diffusion is a random process that can be represented by random walks [11]. The Einstein equation describes the thermal diffusivity K in 3D in the long-time limit (thermal steady state):

$$K = \frac{< \mathbf{R}^2 >}{6 \cdot t}, \tag{1}$$

where $\mathbf{R}$ is the vector displacement of a particle in time t and the Dirac brackets refer to an average over many particle histories. The thermal conductivity λ_i in a phase i is related to the thermal diffusivity K_i in that phase by the expression $K_i = \lambda_i / (\rho_i C_i)$ where ρ_i is the density and C_i the specific heat of phase i. In the case of thermal steady state, it is possible to make use of the Einstein Equation in a Monte Carlo simulation for calculating the relative effective thermal conductivity λ_{eff}/λ_i (λ_i is, for convenience, the maximum thermal conductivity of the individual phases present) by simply and arbitrarily assigning the densities and the specific heats the value of unity in all phases. Then λ_{eff}/λ_i equals the relative effective thermal diffusivity K_{eff}/K_i. Particles are released, one at a time, from randomly chosen sites within the lattice and each is permitted to explore the lattice on a random walk for the same time t. A time step, which is proportional to real time, is an attempt for the particle to jump at a given site. The conductivities of each phase are represented by different jump frequencies Γ (strictly jump probabilities) noting that the thermal diffusion coefficient can be expanded from Eq. (1) as (in 3D):

$$K = \Gamma s^2/6, \tag{2}$$

where s is the jump distance in the lattice. The highest jump frequency is scaled to unity for computational efficiency. Within the relevant temperature range (T < 500 K), the contribution of thermal radiation to the heat transfer is low [12]. Furthermore, the influence of thermal convection is restricted by the low volume fraction of

interconnected porosity in sintered MHSS. Accordingly, the thermal conductivity of the voids is presumed to be zero and the jump frequencies of matrix and inclusion are unity and zero, respectively.

2.2 Finite Element Analysis

For the FE analysis, a meshing algorithm first presented in [13] is applied. Basically, the finite element meshes directly represent the geometry of the material's meso structure (cf. Fig. 1c)). Two constant temperature boundary conditions are prescribed at two opposing surfaces of the calculation model and the arising heat flux is used to calculate the effective thermal conductivity using Fourier's law, see i.e. [9]. By changing the constant temperature planes, the effective thermal conductivity can be determined in three perpendicular directions (i.e. *x*, *y* and *z* direction, cf. Fig. 1). A mesh refinement study of for the finite element meshes used is shown in Fig. 2.

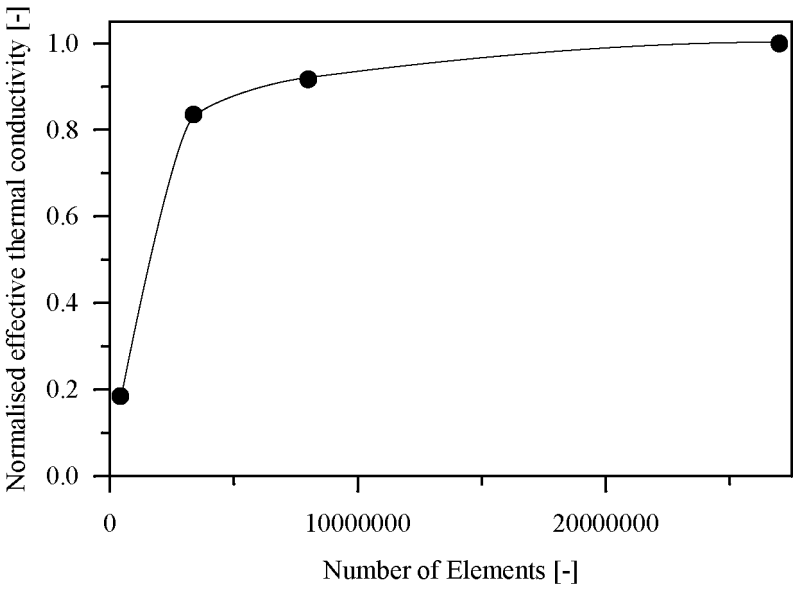

Fig. 2. Mesh refinement analysis of the finite element model.

Four different models with the resolutions 75^3, 150^3, 200^3 and 400^3 elements are considered, where the maximum resolution is limited by computer memory. In addition, the calculation time distinctly increases with increasing mesh density. On the 32–bit system used in the analysis (dual core processor 3.16 GHz, 3.15 GB RAM) the averaged calculation times were 23 sec, 91 sec, 507 sec and 6800 sec for the highest resolution, respectively. It can be observed that accurate convergence is only reached for a high

number of elements and accordingly the highest resolution is chosen for subsequent finite element analyses.

3. Geometry

3. 1 Micro-structure

The first part of the LMC analyses considers the effective thermal conductivity λ_w of the cell wall material. This material parameter is governed by the thermal conductivity λ_s = 16.2 W/(m·K) of the base material steel 316L [14] and its residual porosity. Micro-structural characterisations of sintered MHSS [15] yielded a micro porosity of p = 5.30%. Simple three dimensional lattice models are generated where non-conducting micro-pores are randomly distributed. The fraction of nodes related to micro-pores is thereby identical to the micro porosity. The applied model for porosity presumes that all pores are of similar size and homogeneously distributed. As an alternative, the parameter λ_w can be estimated by a Maxwell-type expression [16], valid for the special case of non-conducting inclusions:

$$\lambda_w = \frac{2(1-p)}{2+p}\lambda_m . \tag{3}$$

3.2 Mesostructure

The second part of the LMC analyses directly addresses the properties of MHSS. The 3D analysis and image acquisition of the hollow structures were carried out using the CT system v|tome|x s of the company: phoenix|X-ray. For the radiography of the samples the microfocus X-ray tube xs|240D with an accelerating voltage of 150 kV and a current of 50 µA was applied. For the 3D volume processing 1000 projections of the 2D radiography images were reconstructed using the datos rec software of phoenix|X-ray. The achieved voxel resolution was 35 µm/voxel. Result of the volume processing was a volume of 650 x 650 x 750 voxel. The 3D visualisation and extraction of the STL-iso-surfaces was applied by using the software Volume Graphics 1.2. An optimised grey value was applied to obtain the best segmentation and separation between the metal structure and air. Based on that grey value the STL-extraction of the iso-surfaces for the following simulation work was performed. The CT images, representing parallel cross sections of the geometry are directly translated to LMC calculation models. The jump frequency assigned to a particular node in a lattice is

144 thereby defined based on the grey-scale value of the corresponding voxel. Figure 1 (b) shows that the metallic phase can be identified by light pixels and voids by dark pixels,
146 respectively. The grey-scale threshold is empirically chosen to match the relative density 9.7% of the MHSS structure [15]. During the LMC model generation the
148 geometry is subdivided into four slightly intersecting sub-volumes in order to investigate local fluctuations of the effective thermal conductivity

150 The FE analyses use calculation models assembled by uniform cubic finite elements [13]. Each finite element represents a subset of voxels of the CT images and analogous
152 to the LMC approach, its thermal conductivity is defined in reference to the grey scale level. However, restrictions in calculation time and computer memory require the
154 bisection of the geometric resolution in the FE models. In a brief comparison, LMC allows for more complex calculation models whilst FE analyses benefits from distinctly
156 lower calculation times.

4. Results

158 The influence of the micro porosity on the effective thermal conductivity of the cell wall material λ_w is shown in Fig. 3. The drawn line corresponds to the analytical solution (3)
160 and is in excellent agreement with corresponding LMC analyses (circles). The porosity of the cell wall material is 5.30% [15] and accordingly the estimated cell wall
162 conductivity λ_w is 14.95 W/(m·K).

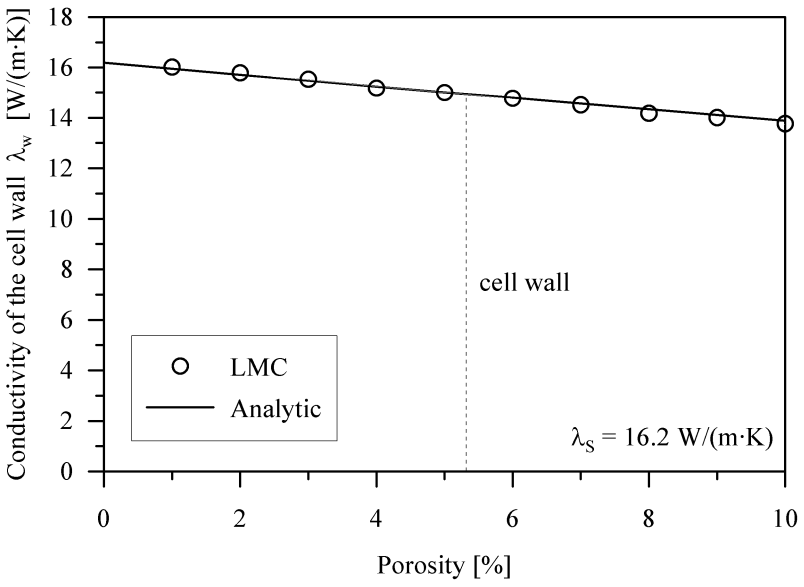

164

Fig. 3. Normalised effective thermal conductivity of the micro structure versus micro porosity.

Using this material parameter as thermal conductivity of the metallic phase identified in the CT scans, LMC and FE analyses are performed on sintered MHSS. As mentioned above, the CT data is subdivided into four sub-geometries in order to investigate local fluctuations of the thermal properties. The results of these analyses are shown in Fig. 4.

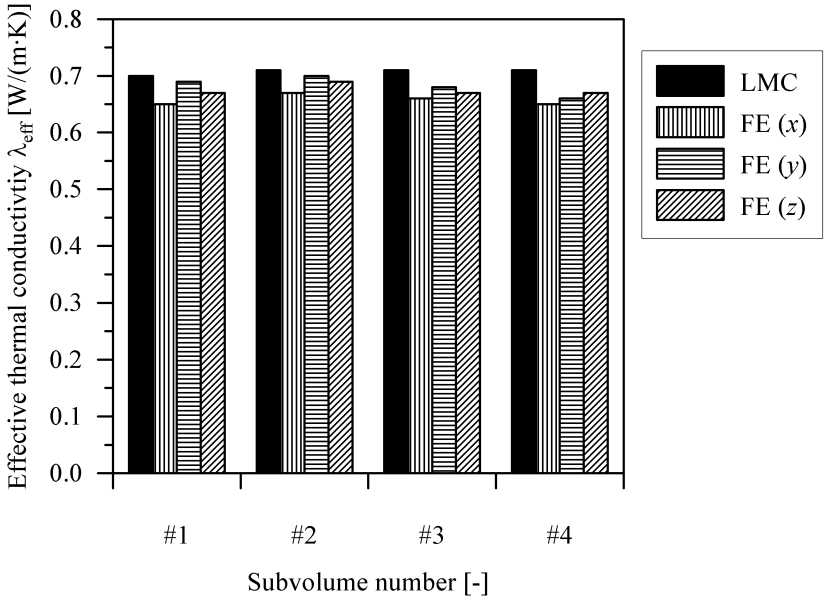

Fig. 4. Effective thermal conductivity of sintered MHSS.

The results of the FE analysis are in good agreement with the LMC findings. The LMC results exhibit circumstantial higher results, which can partially be explained by the superior geometric resolution of the calculation model: the required bisection of the grid resolution (decrease of 650 x 650 x 750 voxels to a total of 325 x 325 x 375 elements) in the FE models might cause the introduction of local 'defects' such as holes in the cell walls that slightly change the FE results. In addition, the results are very similar for all sub-volumes. This is remarkable since the analysed volume elements are relatively small (< 100 spheres) and therefore indicates very homogeneous material properties. Furthermore, the FE results indicate quasi-isotropic thermal properties ($\lambda_x \approx \lambda_y \approx \lambda_z$). The LMC results are average values, blurred over all possible directions. The mean effective thermal conductivities are $\lambda_{\text{eff}} = 0.71$ W/(m·K) (LMC) and $\lambda_{\text{eff}} = 0.67$ W/(m·K) (FE). These values only slightly exceed thermal conductivities (0.57 W/(m·K)) observed for adhesively bonded MHSS [9], which can be explained by the relatively low thermal conductivity of the sintered cell wall material.

Conclusions

This paper addressed numerical analyses on the effective thermal conductivity of sintered Metallic Hollow Spheres Structures. Initially, the effective thermal conductivity of the sintered cell wall material was determined using the LMC method and the results were found to be in excellent agreement with an analytical Maxwell expression. The MHSS analyses were based on CT images and therefore 'real' structures without strong geometric simplifications were considered. The findings of the LMC and FE method were found to be in good agreement; a small deviation can be explained by the superior geometric resolution used in the LMC method. The FE method allowed for the determination of directional conductivities, however, no distinct thermal anisotropy was observed. In addition, the thermal conductivities of four slightly intersecting sub-volumes yielded similar values for relatively small volume elements containing less than 100 spheres each. As a consequence, it can be concluded that sintered MHSS exhibit quasi-isotropic, homogeneous and low effective thermal conductivities.

References

[1] Lopatnikov SL, Gama, BA, Gillespie JW. Int J Impact Eng 2007; 34:587–595.

[2] Golovinand IS, Sinning HR. Mater Sci Eng A 2004; 370:504–511.

[3] Hübelt J, Bingel G. Cellmet News 2006;1:1–2.

[4] Lu TJ, Chen C. Acta Mater (1999); 47:1469–1485.

[5] Fiedler T, Öchsner A, Grácio J, Kuhn G. Mech Compos Mater 2005; 41:405–422.

[6] Ramamurty U, Paul A. Acta Mater 2004; 52:869-876.

[7] Baumeister E, Klaeger S, Kaldos A. J Mater Process Tech 2004; 155–156: 1839-1846.

[8] Fiedler T, Öchsner A. Mater Sci Forum 2007; 553: 45.

[9] Fiedler T, Solórzano E, Öchsner A. Mater Lett 2008; 62: 1204-1207

[10] Fiedler T, Öchsner A, Belova IV, Murch GE, Defect Diffusion Forum 2008; 273-276: 216-221.

[11] Belova IV, Murch GE, Fiedler T, Öchsner A. Diffusion Fundamentals 2007; 4: 15.1-15.23 (e-published).

[12] Lu T, Chen C. Acta Mater 1999; 47:1469.

[13] Fiedler T, Solórzano E, Garcia-Moreno F, Öchsner A, Belova I, Murch G. Mater Sci Eng Tech 2008; accepted for publication.

[14] AK Steel Manufacturer Information 2008; http://www.aksteel.com/pdf/markets_products/stainless/austenitic/316_316L_Data_Sheet.pdf.

[15] Veyhl C; Merkel M; Öchsner A. Defect Diffus Forum 2008; accepted for publication.

[16] J.C. Maxwell: A Treatise on Electricity and Magnetism, Vol. 1 (Clarendon press, Oxford 1892).

Figures Captions

Fig. 1. Geometry of MHSS: a) three dimensional reconstruction of CT data, b) CT cross section used for model generation, c) FE calculation model.

Fig. 2. Mesh refinement analysis of the finite element model.

Fig. 3. Normalised effective thermal conductivity of the micro structure versus micro porosity.

Fig. 4. Effective thermal conductivity of sintered MHSS.